Progress In Electromagnetics Research M, Vol. 100, 213–223, 2021

Quasi-TEM Analysis of Symmetrical Shielded Broadside-Coupled Microstrip Lines

Ali Bououden[1, 2, *], Mohamed L. Riabi[1, 2], Abdelhalim A. Saadi[3], and Mustapha C. E. Yagoub[4]

Abstract—In this work, a numerical quasi-static approach is proposed to efficiently analyze symmetrical shielded broadside-coupled microstrip line (SBCML) structures. Based on the modified least squares boundary residual method combined with a variational technique, this approach allows accurate computation of the electrical/geometrical parameters of different SBCML configurations. The errors for the quasi-TEM electrical parameters range are less than 4%. The proposed technique was demonstrated through successful comparison with data from published works and results obtained from commercial EM simulators like CST-EMS and COMSOL.

1. INTRODUCTION

Broadside-coupled microstrip line (BCML) structures are frequently used in microwave and millimeter-wave (mm-wave) passive/active circuits such as couplers [1, 2], baluns [3, 4], antennas [5], filters [6], phase shifters [7], and impedance transformers [8]. In fact, compared to conventional edge-coupled microstrip lines, such circuits present some enhanced design parameters like tight coupling (3 dB), low VSWR, and low insertion loss. They can also produce equal even- and odd-mode phase velocities. Accurate computation of their quasi-TEM static parameters is essential for successful design of microwave systems, optical integrated circuits, and sensors. During the last years, various works have been devoted to the analysis of shielded/partial shielded and open planar transmission line configurations and to the computation of their quasi-static parameters. Existing quasi-TEM approaches include conformal mapping [9, 10], point matching method [11], neuro-fuzzy [12], method of lines [13], variational method [14, 15], finite element method [16, 17], orthogonal expansion method [18], quasi-static spectral domain method [19], Fourier series expansion [20], and closed-form expression [21]. From that list, the conformal mapping method is one of the most widely used. However, it is valid only over a limited range of physical dimensions and restricted configurations. On the other hand, discretization methods, like the finite element and finite difference time-domain methods, suffer from discretization errors and long CPU time, especially for very thin material layers.

Recently, the quasi-TEM approach has shown several advantages like good convergence rate and accuracy, minimum memory storage and CPU time, while avoiding the need for an expansion function to solve the unknown charge density. Furthermore, it reduces the Gibbs phenomenon effect. Based on the Least Squares Boundary Residual method (LSBR), which has already been successfully and accurately applied to the characterization of multilayer isotropic and anisotropic planar transmission lines with arbitrary geometry for both the quasi-TEM and full-wave modes, the proposed method, called Modified Least Squares Boundary Residual (MLSBR), uses weighting functions (rectangular

Received 27 November 2020, Accepted 26 January 2021, Scheduled 28 January 2021

* Corresponding author: Ali Bououden (bououdenali23@gmail.com).

[1] Laboratoire des Électromagnétismes et Télécommunication, Université de Constantine 1, Route d'Ain El Bey, Constantine 25000, Algérie. [2] Centre de Développement des Technologies Avancées, Algérie. [3] NXP Semiconductors, Suresnes 92150, France. [4] School of Electrical Engineering and Computer Science, University of Ottawa, Ontario K1N 6N5, Canada.

windows) to accelerate the Fourier series convergence [22, 23]. The proposed approach was used for quasi-TEM characterization of different BCML structures such as Shielded Broadside-Coupled Suspended Substrate Microstrip Line (SBSSML), Shielded broadside-coupled Inverted Microstrip-lines (SBIML), and homogeneous Shielded Broadside-coupled Strip Lines (HSBCSL). It was demonstrated through successful comparison with published works as well as data from commercial electromagnetic (EM) simulators.

2. FORMULATIONS AND THEORY

Figure 1 depicts the cross-sectional view of a symmetrical shielded broadside-coupled microstrip line (SBCML) structure. It consists of three isotropic and lossless dielectric layers. The identical top and bottom layers, with a thickness $h1$ and a relative dielectric constant ϵ_{r1}, are separated by a dielectric layer of thickness h and relative dielectric constant ϵ_{r2}. Coupled broadside conductor strips are embedded in the medium layer; they are assumed as perfect conductor with the same width (w) and zero thickness. The structure is enclosed in a perfectly conducting box of width a and height b.

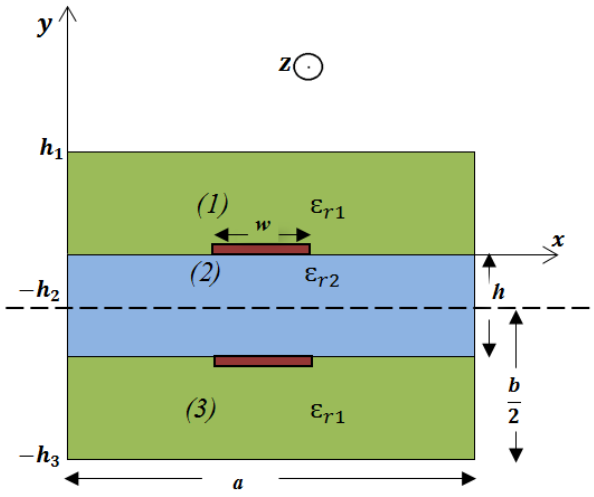

Figure 1. Cross-section view of the symmetric SBCML.

This configuration is assumed uniform and infinite in the z-direction. Because of its symmetry, the structure exhibits two orthogonal propagation modes namely, one odd (Electric Wall — EW) and one even (Magnetic Wall — MW). These two walls are placed at the symmetry plane $y = -h_2$. We also assume that the propagation modes operate in the quasi-TEM regime, i.e., with a propagating wavelength much larger than the cross section widths, and this assumption has been demonstrated in detail [24]. The potential functions of odd and even modes based on a quasi-TEM mode are defined as $\Phi_i^{(o,e)}(x, y)$, where the subscripts "e" and "o" stand for the even and odd modes, respectively. They satisfy the Laplace's differential equation in the 2-D xy-plane:

$$\frac{d^2\Phi_{(i)}^{(o,e)}(x,y)}{dx^2} + \frac{d^2\Phi_{(i)}^{(o,e)}(x,y)}{dy^2} = 0. \tag{1}$$

For the targeted structures, the potentials function can be solved by the method of separation of variables and represented as a sum of truncated Fourier series expansion. So, within each region i ($i = 1$, 2), we have

Region 1: $0 \le x \le a$, $0 \le y \le h1$

$$\Phi_{1m}^{(o,e)}(x,y) = \sum_{m=1}^{m=N} A_m^{(o,e)} \cdot \sinh(p_m(h_1 - y)) \sin(p_m \cdot x) \tag{2}$$

Region 2: $0 \leq x \leq a$; $-h2 \leq y \leq 0$

$$\Phi^{o}_{2m}(x,y) = \sum_{m=1}^{m=N} B^{o}_{m} \cdot \sinh(p_m(y+h_2)) \sin(p_m \cdot x) \tag{3}$$

$$\Phi^{e}_{2m}(x,y) = \sum_{m=1}^{m=N} B^{e}_{m} \cdot \cosh(p_m(y+h_2)) \sin(p_m \cdot x) \tag{4}$$

where, $p_m = mp/a$, N is the number of Fourier series terms, and $A^{(o,e)}_m$ and $B^{(o,e)}_m$ are the unknown coefficients. Note that the coefficients $B^{(o,e)}_m$ can be expressed as function of the unknown coefficients $A^{(o,e)}_m$ by enforcing the continuity potential in the interface at $y = 0$, leading to the following two equations (4)

$$B^{o}_{m} = \left(\frac{\sinh(p_m \cdot h_1)}{\sinh(p_m \cdot h_2)}\right) \cdot A^{o}_{m} \tag{5}$$

$$B^{e}_{m} = \left(\frac{\sinh(p_m \cdot h_1)}{\cosh(p_m \cdot h_2)}\right) \cdot A^{e}_{m} \tag{6}$$

So, we should first determine the coefficients $A^{(o,e)}_m$ by using the MLSBR method as detailed in [22, 23]. Thus, the coefficients $B^{(o,e)}_m$ can be deduced using Eqs. (5) and (6), leading to the odd- and even-mode potential distributions in the two regions while the electric field components for the two modes are given by

$$\overline{E^{(o,e)}_{(i)}}(x,y) = -\overline{\nabla}_T \Phi^{(o,e)}_{(i)}(x,y) \tag{7}$$

$$\overline{D^{(o,e)}_{(i)}}(x,y) = \varepsilon_{(i)} \overline{E^{(o,e)}_{(i)}}(x,y) = -\varepsilon_{(i)} \overline{\nabla}_T \Phi^{(o,e)}_{(i)}(x,y) \tag{8}$$

with $\epsilon_i = \epsilon_0 \epsilon_{ri}$.

2.1. Charge Density and Line Capacitance Per Unit Length

The odd and even charge densities $\rho^{(o,e)}(x,0)$ can be obtained given by applying the Gauss theorem at the interface $y = 0$:

$$\varepsilon_{(1)} \cdot \overline{E_{(y_1)}{}^{(o,e)}}(0,y) - \varepsilon_{(2)} \cdot \overline{E_{(y_2)}{}^{(o,e)}}(0,y) = \rho^{(o,e)}(x,0) \tag{9}$$

The variational expression for the lower bound on odd- and even-mode line capacitances per unit length (p.u.l.) are given by

$$C^{(o,e)} = \frac{Q^{(o,e)2}}{\int_{\frac{(a-w)}{2}}^{\frac{(a+w)}{2}} \rho^{(o,e)}(x,0)\, \Phi^{(o,e)}_{1m}(x,0) dx \int_0^1 dz} \tag{10}$$

with Q being the charge distribution, expressed as

$$Q^{(o,e)} = \int_{\frac{(a-w)}{2}}^{\frac{(a+w)}{2}} \rho^{(o,e)}(x,0)\, dx \int_0^1 dz \tag{11}$$

Note that in this work, the integrals in Eqs. (10) and (11) were evaluated numerically, using the "trapz" function in Matlab.

2.2. Quasi-TEM Electrical Static Parameters

The effective dielectric permittivities of the odd and even modes are given by

$$\epsilon^{(o,e)} = \frac{C^{(o,e)}}{C^{(o,e)}_a} \tag{12}$$

where $C^{(o,e)}$ and $C_a^{(o,e)}$ are the line capacitances per unit length for the odd- and even-modes when the dielectric in the three layers is replaced by air. The phase velocity, odd- and even-mode characteristic impedances as well as the line characteristic impedance can be therefore obtained using the following expressions,

$$v_\rho^{(o,e)} = \frac{c}{\sqrt{\epsilon^{(o,e)}}} \tag{13}$$

$$Z_c^{(o,e)} = \frac{1}{v_\rho^{(o,e)} \cdot C^{(o,e)}} = \frac{1}{c\sqrt{C^{(o,e)} \cdot C_a^{(o,e)}}} \tag{14}$$

$$Z_c = \sqrt{Z_c^{(o)} Z_c^{(e)}} \tag{15}$$

where c is the velocity of the light in free space. Finally, the coupling coefficient is deduced as:

$$C = \frac{z_c^{(0)} - z_c^{(e)}}{z_c^{(0)} + z_c^{(e)}} \tag{16}$$

3. ELECTROMAGNETIC SIMULATION AND MODELING

The electromagnetic (EM) simulation of the symmetric SBCML structure (Figure 1) was performed in both the 3-D CST EMS and 2-D COMSOL EM simulator tools, and these tools are based on the Finite Integration Technique (FIT) and Finite Element Method (FEM), respectively. The modeling and simulation of the proposed structure enables us to extract the capacitance matrix. Note that this matrix should convert to per unit length for the 3-D CST tool. Then, the quasi-static parameters can be computed. The capacitances of the even and odd modes per unit length can be derived from the extracted capacitance matrix coefficients as

$$C^{(o)} = C_{11}^{(d)} + C_{12}^{(d)} \tag{17}$$

$$C^{(e)} = C_{11}^{(d)} - C_{12}^{(d)} \tag{18}$$

where $C_{11}^{(d)}$ and $C_{12}^{(d)}$ are the self- and mutual-capacitances per unit length, respectively. Due to the symmetry of the proposed structure, these parameters are correlated by the following relationships

$$C_{11}^{(d)} = C_{22}^{(d)}, \quad C_{12}^{(d)} = C_{21}^{(d)} \tag{19}$$

A second case was considered in which the dielectric layers were replaced by free space; therefore, the capacitances $C_a^{(o,e)}$ can be calculated using Eqs. (17) and (18).

4. RESULTS

The program codes of the proposed MLSBR and variational techniques have been written in Matlab for both modes on a PC (Intel® i5, 3.30 GHz). The accuracy of the capacitance values depends on the accuracy of the unknown coefficients $A_m^{(o,e)}$ and the number of Fourier terms (N) we consider. Note that the minimum eigenvectors of the least-squares matrix of order ($N \times N$) correspond to the unknown coefficients $A_m^{(o,e)}$. We should also mention that since we used an equivalent circuit model (static capacitive per unit length matrix) of the electro-quasi-static representation described in [4] and [15], the proposed quasi-TEM model is valid when the transverse dimensions are much smaller than wavelength [24]. This can be set in practice by assuming a wavelength at least ten times smaller than the largest distance between two points in the structure. Under this constraint, the currents and charges generated by the electromagnetic fields vary so slowly in time that the electromagnetic fields are practically the same at every instant as if they had been generated by stationary sources [31]. Therefore, we can conclude that the range of validity of our quasiTEM approximation in the lossless case can be determined as follows:

$$a < \frac{\lambda}{10} = \frac{c}{10f\sqrt{\varepsilon_r u_r}} \tag{20}$$

The frequency range can be written as

$$f < \frac{c}{10a\sqrt{\varepsilon_r u_r}} \tag{21}$$

where $u_r = 1$ (nonmagnetic material). The relative dielectric constant ε_r is taken as the maximum value of the different ε_{ri} relative dielectric constants of the structure layers, and c is the light phase velocity of wave in free space. As illustration, for a given structure of parameters $a = 40\,\text{mm}$ and $\varepsilon_r = 2.22$, the validated quasi-TEM model is then valid up to

$$f < \frac{c}{10a\sqrt{\varepsilon_r u_r}} = 10.0673\,\text{GHz} \tag{22}$$

From that, we used the electrostatic solver in both EM simulators COMSOL and CST-EMS at a much lower frequency (2 GHz) to further confirm the validity of our assumptions. The obtained electrical parameters results are accurate within 4% for $\frac{w}{b} \leq 0.4$ and 2% for $0.4 \leq \frac{w}{b} \leq 2$ compared to those obtained by two well-known commercial EM simulators, namely, CST and COMSOL.

In Table 1, we compute the odd- and even-mode line capacitances from inhomogeneous SBCML. Note that the proposed method is faster than EM-simulators tools we used, particularly when the dielectric materials are thin layers. The structure parameters are $a = 2\,\text{mm}$, $b = 16\,\mu\text{m}$, $h = 8\,\mu\text{m}$, $w = 5\,\text{mm}$, $\epsilon_{r1} = 2.22$, $\epsilon_{r2} = 4.75$.

Table 1. Comparison of odd- and even-mode line capacitances and CPU time of symmetric SBCML.

MLSBR			COMSOL			CST-EMS		
$C^{(o)}$ (nF/m)	$C^{(e)}$ (nF/m)	CPU Time	$C^{(o)}$ (nF/m)	$C^{(e)}$ (nF/m)	CPU Time	$C^{(o)}$ (nF/m)	$C^{(e)}$ (nF/m)	CPU Time
7.7172	2.4757	7 sec	7.7751	2.5126	6 min	7.8124	2.5228	8 min

4.1. Example 1: SBSSML

To design a Shielded Broadside-Coupled Suspended Substrate Microstrip Line (SBSSML) structure, we replaced the top and bottom dielectrics layers by air, setting ϵ_{r1} to 1 in Eqs. (7) and (8).

Figure 2 shows the variation of the normalized line charge density distribution on the microstrip conductor $\rho^{(o,e)}(x, 0)$ for odd and even modes, as a function of the normalized abscissa x for the ratio $w/b = 1$. It is apparent that the charge density is almost zero outside the metal conductor region.

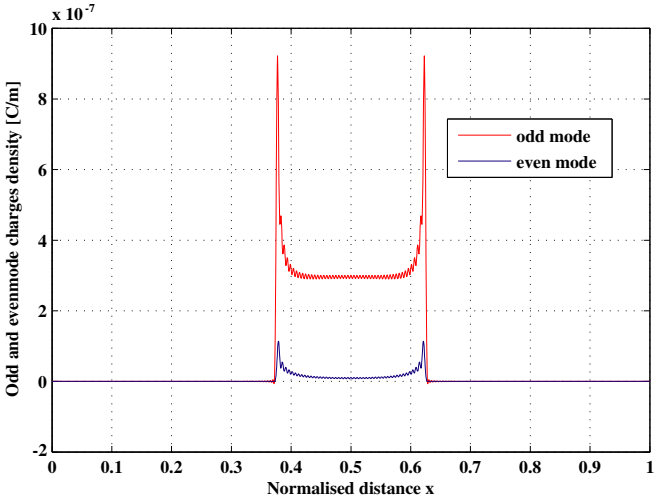

Figure 2. Normalized charge density of SBSSML structure. $a = 4\,\text{mm}$, $b = 1\,\text{mm}$, $h = 0.3b$, $\epsilon_{r1} = 1$, $\epsilon_{r2} = 9.6$.

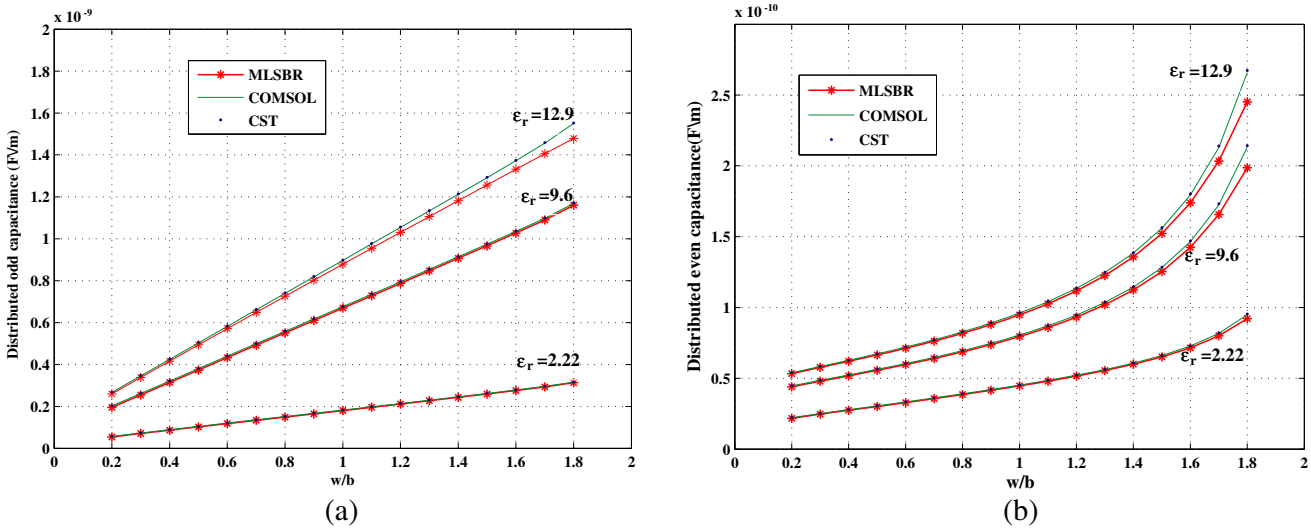

Figure 3. Comparison of capacitance parameter values. (a) Odd mode. (b) Even mode.

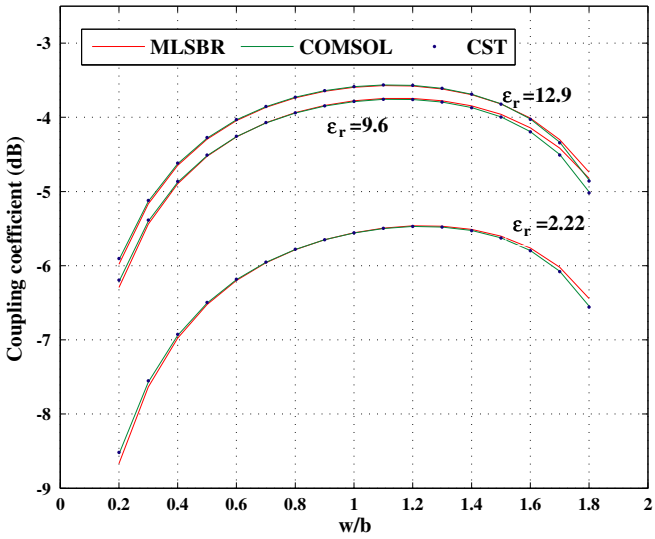

Figure 4. Variation of the coupling coefficient versus the w/b ratio.

Fig. 3 shows the computed line capacitances p.u.l. for the SBSSML configuration for different dielectric substrates as a function of w/b. It is clear that the odd- and even-mode capacitances increase with the increase of either the relative dielectric constant or the w/b ratio ($0.2 \leq w/b \leq 1.8$). We also note that, in this case, the distributed odd capacitance is greater than the even mode capacitance. The maximum error rate of the capacitance is less than 3% than the results obtained from the EM simulators for $\epsilon_r = 12.9$. In Fig. 4, we plot the variation of the coupling coefficient C (dB) of the broadside-coupled strip lines versus the w/b ratio. It can be seen that the coupling coefficient is tightened with decrease of the relative dielectric constant.

Figure 5 depicts the 2D surface potential distributions of SBSSSL obtained in the EM simulators CST EMS and COMSOL.

Computed results of the even- and odd-mode characteristic impedances of the SBCSSML structure were obtained from both the proposed MLSBR approach and the EM-simulators, and then, compared to those obtained from the mentioned techniques as reported in Table 2, we observe that all the obtained data agree well with those from the EM simulators and other approaches.

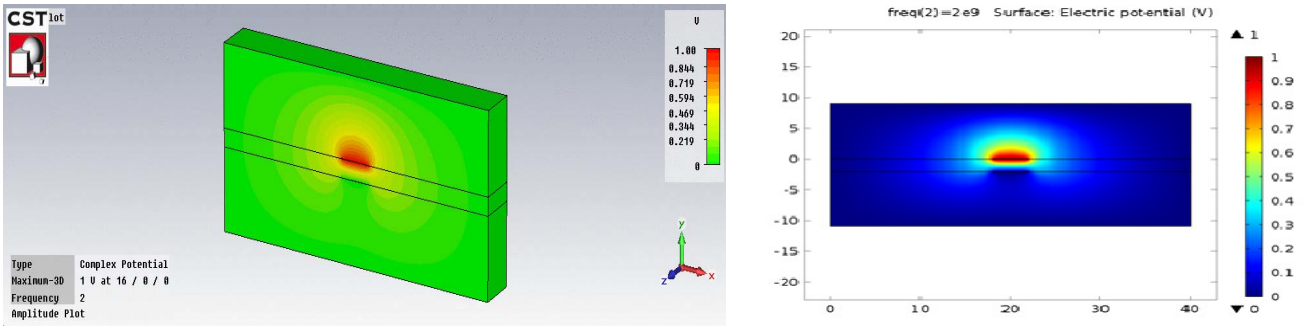

(a) (b)

Figure 5. Surface potential distributions of SBSSML. $a = 40\,\text{mm}$, $b = 20\,\text{mm}$, $h = 2\,\text{mm}$, $w = 2h$, $t = 0.01\,\text{mm}$, $f = 2\,\text{GHz}$, $\epsilon_{r1} = 1$, $\epsilon_{r2} = 2.22$. (a) CST-EMS tool. (b) COMSOL tool.

Table 2. Comparison of odd- and even-mode characteristic impedances of symmetric SBSSML.

w/b	MLSBR		COMSOL		CST		[25]		[26]	
	$z_c^{(o)}\,(\Omega)$	$z_c^{(e)}\,(\Omega)$	$z_c^{(o)}\,(\Omega)$	$z_c^{(e)}\,(\Omega)$	$z_c^{(o)}\,(\Omega)$	$z_c^{(e)}\,(\Omega)$	$z_c^{(o)}\,(\Omega)$	$z_c^{(e)}\,(\Omega)$	$z_c^{(o)}\,(\Omega)$	$z_c^{(e)}\,(\Omega)$
0.1	61.995	269.167	62.611	267.858	61.831	268.321	63.30	274.00	63.80	273.20
0.2	39.982	232.585	39.830	225.564	39.864	226.630	40.50	232.70	40.90	232.20
0.4	23.494	181.886	23.354	175.434	23.367	176.201	24.00	182.20	23.93	181.20
0.6	16.661	149.056	16.571	144.074	16.577	14..676	17.00	152.50	16.95	150.00
0.8	12.911	125.765	12.848	121.884	12.854	122.397	13.50	130.10	13.62	128.00
1	10.538	108.068	10.492	104.955	10.496	105.399	-	-	10.70	112.99

Table 3 reports the odd- and even-mode characteristic impedance values for different values of strip lines widths w/h of the shielded BCSSML structure. They can be usefully compared to those reported in published works.

Table 3. Comparison of the odd- and even-modes characteristic impedances of SCBSSML structure. $a = 4\,\text{mm}$, $b = 1\,\text{mm}$, $\epsilon_r = 9.6$.

w/h	MLSBR		CST		Kumar [27]		Bhat & Koul [29]		COMSOL [28]	
	$z_c^{(e)}\,(\Omega)$	$z_c^{(o)}\,(\Omega)$	$z_c^{(e)}\,(\Omega)$	$z_c^{(o)}\,(\Omega)$	$z_c^{(e)}\,(\Omega)$	$z_c^{(o)}\,(\Omega)$	$z_c^{(e)}\,(\Omega)$	$z_c^{(o)}\,(\Omega)$	$z_c^{(e)}\,(\Omega)$	$z_c^{(o)}\,(\Omega)$
0.2	190.52	20.70	189.36	20.20	187.31	21.62	186.05	21.79	190.07	18.57
1	99.89	5.32	102.35	5.30	98.01	5.352	99.85	5.393	93.76	4.78
2	63.45	2.77	65.01	2.76	61.947	2.770	63.68	2.784	61.02	2.488

4.2. Example 2: Shielded Broadside-Coupled Inverted Microstrip Lines (SBIML)

In this section, a shielded broadside-coupled inverted microstrip line (SBIML) structure was analyzed. As depicted in Fig. 6, it is constituted of two top and down dielectric layers spaced by air. The broadside microstrip lines are inside the air layer. Note that the thickness of the microstrip line conductors has been assumed zero. Tables 4 and 5 summarize the quasi-TEM parameters associated with that structure. These are derived from the proposed technique and compared to those from EM-simulations carried out with CST and COMSOL, as well as to those in [29], for various w/b and h/b ratios. The physical parameters of this topology are $a = 40w$, $b = 20\,\text{mm}$, $\epsilon_r = 2.22$. Through the results presented in these

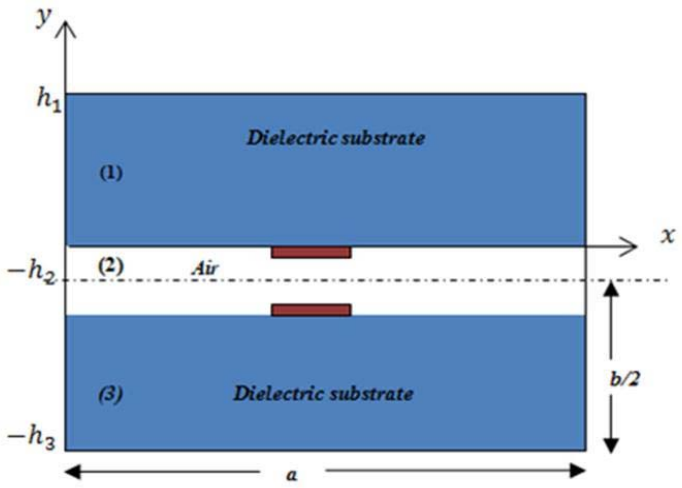

Figure 6. Cross-section view of Shielded Broadside-coupled Inverted Microstrip Lines (SBIML).

Table 4. Computed characteristic impedances of symmetric SBIML.

h/b	w/b	MLSBR		CST		COMSOL		Bhat & Koul [29]	
		$z_c^{(o)}$ (Ω)	$z_c^{(e)}$ (Ω)	$z_c^{(o)}$ (Ω)	$z_c^{(e)}$ (Ω)	$z_c^{(o)}$ (Ω)	$z_c^{(e)}$ (Ω)	$z_c^{(o)}$ (Ω)	$z_c^{(e)}$ (Ω)
0.1	0.4	32.76	138.93	29.424	128.533	30.212	130.547	31.01	132.35
	0.8	18.69	95.74	16.563	87.164	17.117	89.219	17.54	90.93
	1.2	13.13	73.10	11.554	66.169	11.953	67.894	12.23	69.42
	1.6	10.15	59.10	8.832	52.944	9.183	54.802	9.39	56.13
	2	8.29	49.57	7.070	44.015	7.456	45.944	7.61	47.09
0.3	0.4	59.29	109.84	53.971	102.082	55.202	103.869	56.30	105.15
	0.8	36.02	75.26	32.349	68.775	33.342	70.544	34.07	71.70
	1.2	25.89	57.23	23.009	51.732	23.898	53.471	24.42	54.49
	1.6	20.22	46.14	17.632	41.131	18.623	43.054	19.02	43.96
	2	16.61	38.65	14.663	34.702	15.256	36.035	15.57	36.83

tables relating to the analysis of the SBISL structure, it can be noted that they are very close to those of the Bhat & Koul method [29], which once again proves the effectiveness and accuracy of the presented approach.

4.3. Example 3: Homogeneous Shielded Broadside-Coupled Strip Lines (HSBCSL)

A homogeneous SBCSL (HSBCSL) structure was also investigated. For this aim, we replaced all the dielectric layers in Figure 1 by homogeneous dielectric layers (with $\epsilon_{r1} = \epsilon_r$). Several papers have been issued regarding the calculation of the quasi-TEM mode propagation parameters for homogeneous SBCSL structures like [29] and [30]. These published data were computed from closed formula expressions derived from the conformal mapping method. However, they were valid only for a w/h ratio which is greater than 0.35. Our approach enabled finding the quasi-TEM electrical parameters with arbitrary w/h ratios. Tables 6 and 7 depict the quasi-TEM static parameters results of the

Table 5. Comparison of characteristic impedance and coupling coefficients data of symmetric SBIML.

h/b	w/b	MLSBR		CST		COMSOL		Bhat & Koul [29]	
		$Zc\,(\Omega)$	$C\,(\mathrm{dB})$	$Zc\,(\Omega)$	$C\,(\mathrm{dB})$	$Zc\,(\Omega)$	$C\,(\mathrm{dB})$	$Zc\,(\Omega)$	$C\,(\mathrm{dB})$
0.1	0.4	67.469	−4.1755	61.498	−4.0486	62.802	−4.0944	64.063	−4.1472
	0.8	42.311	−3.4367	37.996	−3.3417	39.078	−3.374	39.936	−3.3934
	1.2	30.992	−3.1563	27.650	−3.0647	28.488	−3.0906	29.137	−3.0927
	1.6	24.495	−3.0147	21.625	−2.9255	22.434	−2.9389	22.957	−2.9337
	2	20.272	−2.9324	17.640	−2.8148	18.508	−2.8444	18.930	−2.8322
0.3	0.4	80.705	−10.4898	74.2262	−10.2204	75.722	−10.2872	76.941	−10.383
	0.8	52.068	−9.0537	47.167	−8.8688	48.499	−8.9199	49.424	−8.9765
	1.2	38.498	−8.4731	34.500	−8.3065	35.747	−8.3534	36.478	−8.3799
	1.6	30.553	−8.1675	26.9300	−7.9611	28.316	−8.0438	28.915	−8.0461
	2	25.338	−7.9837	22.557	−7.8312	23.447	−7.8484	23.946	−7.8353

Table 6. Computed characteristic impedances of symmetric HSBCSL.

w/h	**MLSBR**			**CST**			**COMSOL**		
	$z_c^{(e)}\,(\Omega)$	$z_c^{(o)}\,(\Omega)$	$z_c\,(\Omega)$	$z_c^{(e)}\,(\Omega)$	$z_c^{(o)}\,(\Omega)$	$z_c\,(\Omega)$	$z_c^{(e)}\,(\Omega)$	$z_c^{(o)}\,(\Omega)$	$z_c\,(\Omega)$
0.2	203.488	121.415	157.183	192.895	113.177	147.754	193.775	114.054	148.663
0.3	184.647	103.535	138.266	177.059	97.837	131.616	177.863	98.6126	132.437
0.4	171.953	91.581	125.490	165.844	87.241	120.285	166.391	87.777	120.852
0.5	162.035	82.522	115.635	156.956	79.158	111.464	157.332	79.504	111.841
0.6	153.863	75.372	107.689	149.367	72.508	104.069	149.785	72.873	104.477
0.7	146.971	69.526	101.086	142.950	67.109	97.945	143.272	67.387	98.258
0.8	140.835	64.578	95.367	137.241	62.538	92.643	137.509	62.744	92.887
0.9	135.411	60.372	90.416	132.023	58.525	87.902	132.318	58.748	88.167

Table 7. Effective dielectric constants and coupling coefficient of symmetric HSBCSL.

w/h	**MLSBR**			**CST**			**COMSOL**		
	C (dB)	$eff^{(o)}$	$eff^{(e)}$	**C (dB)**	$eff^{(o)}$	$eff^{(e)}$	**C (dB)**	$eff^{(o)}$	$eff^{(e)}$
0.2	−11.9510	2.3494	2.3591	−11.6854	2.35	2.35	−11.7347	2.3500	2.3500
0.3	−11.0116	2.3531	2.3583	−10.8064	2.35	2.35	−10.8530	2.3500	2.3500
0.4	−10.3147	2.3534	2.3618	−10.1566	2.35	2.35	−10.1924	2.3500	2.3500
0.5	−9.7588	2.3510	2.3574	−9.6431	2.35	2.35	−9.6663	2.3499	2.3499
0.6	−9.3092	2.3524	2.3582	−9.2083	2.35	2.35	−9.2329	2.3499	2.3499
0.7	−8.9292	2.3507	2.3572	−8.8487	2.35	2.35	−8.86853	2.3499	2.3499
0.8	−8.6069	2.3511	2.3562	−8.5442	2.35	2.35	−8.5576	2.3499	2.3499
0.9	−8.3298	2.3505	2.3571	−8.2746	2.35	2.35	−8.2897	2.3499	2.3499

HSBCSL topology. A close agreement was found with simulated data using CST and COMSOL tools for various w/h ratios ($0.2 \leq w/h \leq 0.9$). The symmetric HSBCSL parameters are $a = 500\,\mathrm{mil}$, $b = a$, and $\epsilon_r = 2.35$.

5. CONCLUSION

A hybrid quasi-TEM technique was proposed, based on the MLSBR and variational approaches for an accurate computation of quasi-TEM static parameters of generic symmetric shielded broadside-coupled microstrip line structures. It was demonstrated through the design of different SBCML configurations and the numerical results obtained for both the odd- and even-mode excitations successfully compared to those from the technical literature as well as to those from commercial EM simulators. The approach can be applied to asymmetric multilayer coupled microstrip structures.

REFERENCES

1. Grys, D. B., R. Storch, and T. Musch, "A multisection ultra wideband directional coupler in multilayer broadside coupled stripline technology," *IEEE Microwave Conf.*, 39–42, Bochum, Germany, 2016.
2. Kim, I. B., S. K. Kim, W. Mohyuddin, H. C. Choi, and K. W. Kim, "Design of wideband directional couplers using three types of broadside coupled-lines," *IEEE Int. Symp. on Antennas and Propag.*, 932–933, Okinawa, Japan, 2016.
3. Kim, S. G. and K. Chang, "Ultrawide-band transitions and new microwave components using double-sided parallel-strip lines," *IEEE Trans. Microw. Theory Tech.*, Vol. 52, No. 9, 2148–2152, 2004.
4. Moghaddam, E. S. and A. Ahmadi, "180° hybrid using a novel planar balun on suspended substrate for beam forming network applications," *Int. J. RF Microw. Comput.-Aided Eng.*, No. 9, e22280, 2020.
5. Huang, K. F. and C. K. Tzuang, "Characteristics and design of broadside-coupled transmission line at a higher order leaky mode," *IEEE Trans. Microw. Theory Tech.*, Vol. 51, No. 2, 440–447, 2003.
6. Lin, S., H. Cui, L. Wu, W. Wang, and X. Sun, "Design of broadside-coupled parallel line millimetre-wave filters by standard 0.18-μm complimentary metal oxide semiconductor technology," *IET Microw. Antennas Propag.*, Vol. 6, No. 1, 72–78, 2012.
7. Abbosh, A. M., "Ultra-wideband phase shifters," *IEEE Trans. Microw. Theory Tech.*, Vol. 55, No. 9, 1935–1941, 2007.
8. Winslow, T. A., "A novel broadside coupler model for MMIC impedance transformer design," *IEEE 41st European Microwave Conf.*, 309–312, Manchester, UK, 2011.
9. Wong, M. F., V. F. Hanna, O. Picon, and H. Baudrand, "Analysis and design of slot-coupled directional couplers between double-sided substrate microstrip lines," *IEEE Trans. Microw. Theory Tech.*, Vol. 39, No. 12, 2123–2129, 1991.
10. Abbosh, A. M., "Analytical closed-form solutions for different configurations of parallel-coupled microstrip lines," *IET Microw. Antennas Propag.*, Vol. 3, No. 1, 137–147, 2009.
11. Zhu, N. H., W. Qiu, Y.-B. Pun, and P.-S. Chung, "Analysis of two-layer planar transmission lines with the point matching method," *Int. J. Eletron.*, Vol. 80, No. 1, 99–105, 1996.
12. Übeyli, E. D. and İ. Güler, "Adaptive neuro-fuzzy inference system to compute quasi-TEM characteristic parameters of microshield lines with practical cavity sidewall profiles," *Neurocomputing*, Vol. 70, Nos. 1–3, 296–304, 2006.
13. Zitouni, A., H. Bourdoucen, and T. Nait Djoudi, "Quasi-static MoL-based approach for the analysis of multilayer transmission line structures," *The International Journal of Numerical Modelling: Electronic Networks, Devices and Fields*, Vol. 10, No. 4, 209–216, 1997.
14. Yamashita, E. and K. Atsuki, "Strip line with rectangular outer conductor and three dielectric layers," *IEEE Trans. Microw. Theory Tech.*, Vol. 18, No. 5, 238–244, 1970.
15. Liu, J., J. Yang, and A. U. Zaman, "Analytical solutions to characteristic impedance and losses of inverted microstrip gap waveguide based on variational method," *IEEE Trans. Microw. Theory Tech.*, Vol. 66, No. 12, 7049–7057, 2018.

16. Pantic-Tanner, Z., G. Mavronikolas, and R. Mittra, "A numerical absorbing boundary condition for quasi-TEM analysis of microwave transmission lines using the finite-element method," *Microw. Opt. Technol. Lett.*, Vol. 9, No. 3, 134–136, 1995.
17. Musa, S. M. and M. N. Sadiku, "Finite element approach of shielded, suspended and inverted microstrip lines," *Bull. Electr. Eng. Inform.*, Vol. 2, No. 1, 1–10, 2013.
18. Xiao, F., M. Norgren, and S. He, "Quasi-TEM approach of coupled-microstrip lines and its application to the analysis of microstrip filters," *Int. J. RF Microw. Comput.-Aided Eng.*, Vol. 22, No. 1, 131–139, 2012.
19. Tran, M. and C. Nguyen, "Modified broadside-coupled microstrip lines suitable for MIC and MMIC applications and a new class of broadside-coupled band-pass filters," *IEEE Trans. Microw. Theory Tech.*, Vol. 41, No. 8, 1336–1342, 1993.
20. Khalaj-Amirhosseini, M., "Determination of capacitance and conductance matrices of lossy shielded coupled microstrip transmission lines," *Progress In Electromagnetics Research*, Vol. 50, 267–278, 2005.
21. Tomar, R., Y. M. Antar, and P. Bhartia, "Computer-aided-design (CAD) of suspended-substrate microstrips: An overview," *Int. J. RF Microw. Comput.-Aided Eng.*, Vol. 15, No. 1, 44–55, 2005.
22. Riabi, M. L., M. Ahmadpanah, H. Benzina, H. Baudrand, and V. FouadHanna, "Performance of the MLSBR using efficient weighting functions for planar structures," *IET Microw. Antennas Propag.*, Vol. 142, No. 4, 364–368, 1995.
23. Sakli, H., H. Benzina, T. Aguli, and J.-W. Tao, "A rigorous study of some planar structures with longitudinally magnetized ferrite by a modified LSBR method," *International Journal of Microwave and Optical Technology*, Vol. 4, 358–367, 2009.
24. Horno, M., F. L. Mesa, F. Medina, and R. Marques, "Quasi-TEM analysis of multilayered, multiconductor coplanar structures with dielectric and magnetic anisotropy including substrate losses," *IEEE Trans. Microw. Theory Tech.*, Vol. 38, No. 8, 1059–1068, 1990.
25. Bahl, I. J. and P. Bhartia, "Analysis of broadside coupled microstriplines," *Arch. Elek. Ubertragung.*, Vol. 34, No. 5, 223–226, May 1980.
26. Bhartia, P. and P. Pramanick, "Computer-aided design models for broadside-coupled striplines and millimeter-wave suspended substrate microstrip lines," *IEEE Trans. Microw. Theory Tech.*, Vol. 3, No. 11, 1476–1481, 1988.
27. Kumar, R., "Design model for broadside-coupled suspended substrate stripline for microwave and millimeter-wave applications," *Microw. Opt. Technol. Lett.*, Vol. 42, No. 4, 328–331, 2004.
28. Musa, S. M. and M. N. Sadiku, "Modeling of shielded broadside-coupled substrate striplines," *Microw. Opt. Technol. Lett.*, Vol. 51, No. 1, 9–13, 2009.
29. Bhat, B. and S. K. Koul, *Stripline Like Transmission Lines for Microwave Integrated Circuits*, 332–961, Wiley, New York, 1989.
30. Staszek, K., K. Wincza, and S. Gruszczynski, "Rigorous approach for design of differential coupled-line directional couplers applicable in integrated circuits and substrate-embedded networks," *Nature Scientific Reports*, Vol. 6, 25071, 2016.
31. https://doc.comsol.com/5.4/doc/com.comsol.help.acdc/ACDCModuleUsersGuide.pdf.